BIAXIAL MECHANICAL CHARACTERIZATION OF PORCINE PERIOSTEUM

by

PHILLIP DANIEL WARREN

Presented to the Faculty of the Graduate School of

The University of Texas at Arlington in Partial Fulfillment

of the Requirements

for the Degree of

MASTER OF SCIENCE OF BIOMEDICAL ENGINEERING

THE UNIVERSITY OF TEXAS AT ARLINGTON

May 2008

ACKNOWLEDGEMENTS

I would like to thank my supervising professor Dr. Paul Wells for allowing me to study under him and to learn from his experience not just as an engineer, but as an individual thinker. I wish to thank my academic advisor Dr. Cheng-Jen Chuong, as my primary teacher of biomechanics and proper scholarly etiquette. I wish also to thank Dr. Robert Eberhart for taking an interest and serving in my defense committee.

Furthermore, I am indebted to Texas Scottish Rite Hospital for Children, for providing all the necessary equipment and connections for completing this research, as well as the University of Texas Southwestern Medical Center for research specimens.

I am tremendously appreciative to all the teachers who taught me throughout school, at the Georgia Institute of Technology, at Torrington, and finally at the University of Texas at Arlington. I would especially like to thank Drs. Thomas Burkholder and Mindy L. Millard-Stafford for encouraging and enabling me to pursue academic advancement outside of mechanical engineering.

Finally, I would like to thank my sister who has motivated me throughout all of my studies, from grade school to my new school. I am extremely thankful to my mother and father for their economic and emotional support, as well as their sense of humor. I am also immensely grateful for my friends.

April 17, 2008

ABSTRACT

BIAXIAL MECHANICAL CHARACTERIZATION

OF PORCINE PERIOSTEUM

PHILLIP DANIEL WARREN, M.S.

The University of Texas at Arlington, 2008

Supervising Professor: Paul B. Wells

Periosteum is multipotent tissue responsible for cortical bone deposition and is important in fracture repair. Research indicates the periosteum is mediated by similar mechanical signals to those that mediate bone growth and remodeling. Therefore, biaxial mechanical characterization of periosteum can be very informative, indeed. This paper presents the results of the first such examination. The porcine periosteum herein has at least three distinct layers – a cellular layer, an elastin-rich layer, and a collagen-rich layer – the latter two providing structural integrity. Not surprisingly then, the general biaxial mechanical characteristics of periosteum resemble those of other collagen and/or elastin-rich membranes. That is, periosteum is non-linear, anisotropic, and transitions from an easily-extensible state to near-inextensibility over a narrow

range of stretch, with the circumferential direction being the least extensible relative to the traction-free configuration. Tissues are qualitatively similar across all pigs and anatomical sites tested herein, suggesting one may somewhat indiscriminately pool periosteal samples from multiple pigs and multiple locations, within the limits tested herein, for a common parametric analysis. Tissue shrinkage was significantly more pronounced in the axial direction when removed from the bone, corresponding well to the dense population of elastin fibers oriented in that direction. Finally, a seven-parameter pseudo-strain energy function was investigated to model our data and found to fit well, but exhibited poor predictive capacity.

TABLE OF CONTENTS

LIST OF ILLUSTRATIONS

LIST OF TABLES

CHAPTER 1

INTRODUCTION

1.1 Ilizarov Device

The use of the Ilizarov device and callotasis for treating limb length discrepancies, improper bone union, and obstructive bone curvature is documented well [Herring, 2002; Orwoll, 2003; Skerry, 2006]. Complications, reported by Tachjidans, range from 14% [De Bastiani, 1987] to 134%, indicating more than one complication [Noonan, 1998], including infection, tissue mechanical damage (e.g. scarring), premature or delayed consolidation, and poor quality regenerate. The potential sequelae can be devastating both physically and emotionally, and therefore research to improve such procedures remains paramount. Specifically, we must improve our understanding of the mechanobiological processes that govern bone modeling and remodeling, particularly in response to therapeutically-applied mechanical loads.

1.1.1 Ilizarov Procedure

The Ilizarov method for limb-lengthening is grossly unchanged since its inception in the 1950's. The general method consists of an osteotomy, placement of a fixator, a latency period of five to seven days during which a fracture callus forms, periodic distraction (lengthening), a consolidation period during which the new bone ossifies, and removal of the fixator. In a typical lengthening protocol a patient's device

is distracted 1 mm per day in conjunction with cyclic micromotion as the patient ambulates [Paley et al., 1992]. Compressive loads are transmitted through the fixator, while applied tensile loads are shared by various tissues (skin, nerves, vasculature, fracture callus, etc). There are few customizations of the procedure, despite the likelihood of multiparametric variations from patient to patient that could result in dramatically different stresses and/or stretches within the affected tissues, thereby eliciting different mechanobiological responses.

1.2 Periosteum

Though all of the affected tissues likely contain mechanosensitive elements, the periosteum is of particular interest in limb-lengthening due to its population of osteoprogenitor cells and established role in fracture repair [Sakata et al. 2006; Ringe et al., 2002; Sencimen et al., 2007]. Details of periosteal anatomy and biology have been described well [Squier et al., 1990; Parfitt, 1994; Carter et al., 1998; Seeman, 2003; Allen et al., 2004; Seeman, 2007]. Correspondingly, the complexity of this multipotent tissue has been illuminated through the close examination of the chondrogenic and osteogenic potential. More specifically, experiments were carried out with a focus at the cellular level [Brighton et al., 1992; Price et al., 1994; Hoshi et al., 1999], the genetic level [Hughes et al., 1995; Horiuchi et al., 1999; Rios et al., 2005; Kuroda et al., 2005; Hankenson et al., 2006], and the molecular level [Robins, 1994; Chenu et al., 1994; Volpin et al., 1986; Radomsky et al., 1998; Einhorn, 1998; Lieberman et al., 2002; Termaat et al., 2005; Malizos et al., 2005]. Furthermore, studies were conducted spotlighting controlled medias [Harris et al., 1994; Solchaga et al., 1998], sex hormones

[Vanderschueren et al., 2006], gender [Balena et al., 1992], age [Epker et al., 1966; O'Driscoll et al., 2001; Meyer et al., 2007], mortality [O'Driscoll et al., 1999], and simulations [Matziolis et al., 2006]. Applications of this data can be seen in tissue engineering experiments demonstrated in collagen matrices [Ignatius et al., 2005], PLGA scaffolds [Zheng et al., 2006], and transplants [Tsubota et al., 1999; Agata et al., 2007].

1.2.1 Periosteal Anatomy

Briefly, the periosteum is a thin membrane that envelopes cortical bone and is comprised of an outer fibrous layer and an inner cellular layer (the cambium). The fibrous layer is primarily type I collagen, with some elastin, and provides physical support for fibroblasts, vasculature, nerves, and the underlying cambium. The cambium is comprised of osteoprogenitor cells, and is responsible for the regulation of circumferential growth through intramembraneous cortical deposition and resorption [Raisz, 1984]. The periosteum transitions to more specialized anatomy at certain locations resulting in spatial and physiological variations, leading to profound disparities in mechanical properties. Key to predicting the response of periosteum to mechanical loads is better understanding of its mechanical behavior [Henderson et al., 2002].

1.2.1.1 Periosteal Mechanical Studies

Studies on the mechanics of bone and periosteum have been conducted under several types of loading criteria including brief loading [Pead et al., 1988], compression and distraction [Wilson-MacDonald et al., 1990], relaxation [Warrell et al., 1979;

Simon et al., 2003], elevation [Kesseler et al., 2007], *in vivo* loading [Ellender et al., 1989], and simulations of surface loading [Carpenter et al., 2007]. Additional studies have focused on the gene upregulation post-mechanical stimulus [Jones et al., 1991; Raab-Cullen et al., 1994]. Soft tissue mechanical studies have been uniaxial in nature and focused primarily on failure strength [Uchiyama et al., 1998; Popowics et al., 2002]. However, none of these loading criterias, nor uniaxial analyses, nor mechanical loading to failure reflects typical *in vivo* conditions.

1.2.2 Focus

We developed an experimental device and methodology that allows us to characterize, for the first time, the biaxial mechanics of freshly excised periosteal tissue, and to monitor alterations in the mechanical behavior as the periosteum is cultured under well-controlled dynamic and/or static mechanical constraints. This paper focuses on the former.

CHAPTER 2

METHODS

2.1 The Device

A custom-designed biaxial testing device was adapted from a similar device presented in [Humphrey et al., 2007]. Because results from herein will be extended to living tissues, care was taken to make the chamber biocompatible, autoclavable, environmentally sealed, oxygen-perfusable, and compact enough to fit on the stage of an inverted microscope.

2.1.1 Chamber

Except where noted, the chamber assembly is constructed from polycarbonate. A 7 x 7-inch cruciform chamber was constructed from solid stock. At the center of the chamber, a 1 x 1-inch hole is covered with a quartz-glass cover slip, allowing inverted light microscopy. Two stainless steel push rods penetrate the end of each cruciform arm through J-type roulon sleeve bearings (McMaster Carr), and are connected outside the chamber by a push plate and inside the chamber by a tissue mount assembly. The assembly consists of a mount plate to which a vertical beam-type thin-film load cell (one per axis; Strain Measurement Devices, Inc) or polycarbonate beam is attached. A suture bracket is attached to the free end of the beam. Each bracket is pre-strung with continuous 6-0 silk suture looped through four holes to facilitate attachment of the tissue. The top edge of the chamber is lined with a custom-cut silicone gasket, creating

a seal with the magnetically-attached lid. For mechanical testing, the chamber fits atop a custom-designed testing platform, pictured in Figure 2.1.

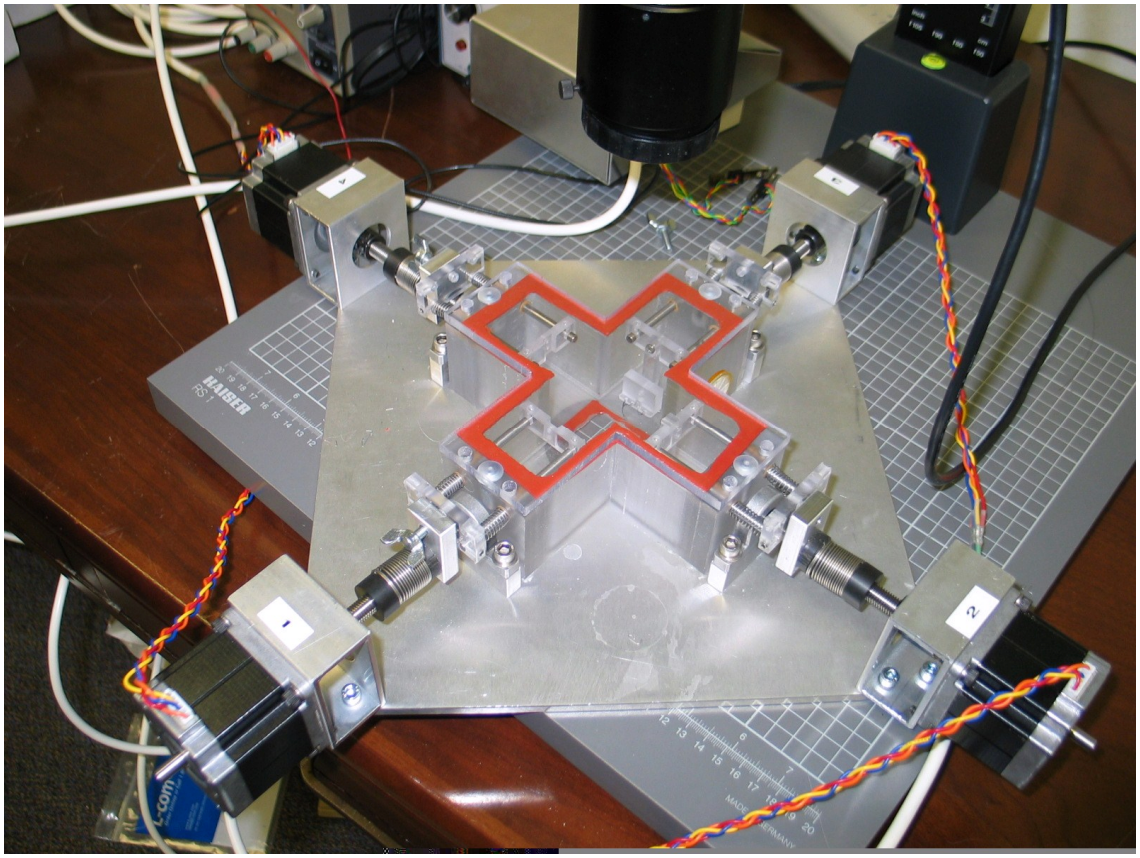

Figure 2.1 Overhead view of assembled chamber on the platform.

2.1.2 Platform

The platform has four orthogonally-opposed translation units, each comprised of a size 23 stepper motor (US Digital) linked in-line to a 3/8-inch lead screw/nut assembly (0.05in lead; Kerk Motion). Attached to each nut is an aluminum plate that connects easily to a push plate on the chamber using a single thumb-screw. The motors are interfaced via a PCI7350 computer controller (National Instruments) to a custom-coded LabVIEW program, described below. The controller/motor combination allows

for 50,000 steps per revolution, thus yielding a translation resolution of approximately 0.03μm per step when used with the aforementioned lead screw.

2.1.2.1 Video Capture System

The platform sits atop an RS-1 copy table (Kaiser) to perform non-contact video monitoring of tissue deformation [Humphrey et al., 1987]. The video capture system is comprised of an AVT Guppy FireWire camera fitted with a Navitar Zoom 7000 lens and mounted to the elevator column of the copy table. At maximum zoom, one may view a 4 x 6mm field in the central region of the tissue. The platform and tissue are monitored by a video capture system.

2.1.3 Computer Control and Error Analysis

Our code is capable of manual, independent control of each motor or a near-infinite combination of automated biaxial motor movements based on either load or displacement feedback. Outputs from the load cells are conditioned and amplified using a custom breadboard circuit, and then input to the computer via a USB-6009 digital acquisition board [National Instruments]. Unique calibration parameters are used for each load cell to convert the output to mass, with a resolution of 0.03g. Video is fed into LabVIEW through a direct IEEE1394 (firewire) interface. Pixel coordinates of each marker's centroid are determined at 30Hz via a search algorithm based on pixel intensity values [Downs et al., 1990], from which a deformation field is calculated using bilinear isoparametric interpolation. Trials revealed that locations of the centroids varied by ± one pixel between multiple measurements on a static image, representing a maximum displacement error of only ± 0.017% for markers separated 1mm. In some

cases, the tissue was noted to move through different focal planes as it was stretched or relaxed. To evaluate whether this change in object distance created an apparent change in tissue deformation, we sampled data from a single tissue as the camera was adjusted from far-range out-of-focus, to in-focus, and then to near-range out-of-focus. Apparent changes in the centroid locations were small, resulting in a 0.7% change in displacement calculations from one extreme of the focal range to the other. A schema of this system is shown below in Figure 2.2.

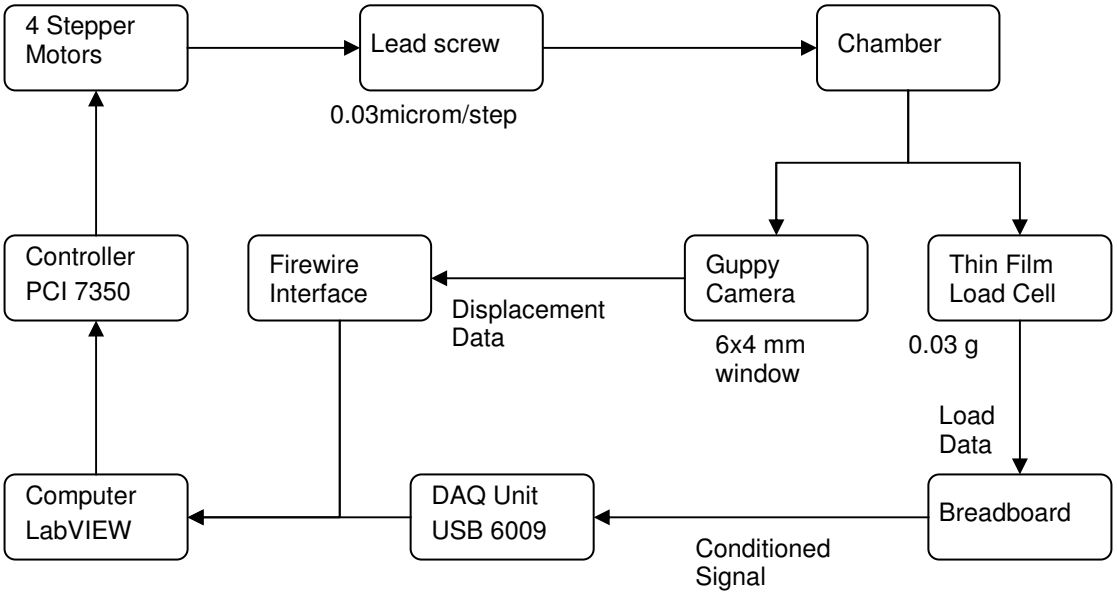

Figure 2.2 Schematic representing the experimental setup.

2.2 Tissue Preparation

2.2.1 Excision

Sacrificing pigs for the sole purpose of harvesting periosteum was not easily justified. Therefore, we harvested tissues from non-survival pigs used in other studies.

Three pieces of periosteum (~ 15mm x 15mm) were harvested within one hour of sacrifice and under aseptic conditions from the medial ulna diaphysis of pigs, bilaterally, yielding six pieces of tissue from each pig. Tissue dimensions were measured with digital calipers and the longitudinal axis was demarcated before removal from the bone, aided by a periosteal elevator. The location of each tissue was also recorded, based on proximity to the elbow, as proximal, medial, or distal (Figure 2.3). Tissues were stored in cold saline prior to mechanical testing or histological analysis by hospital staff.

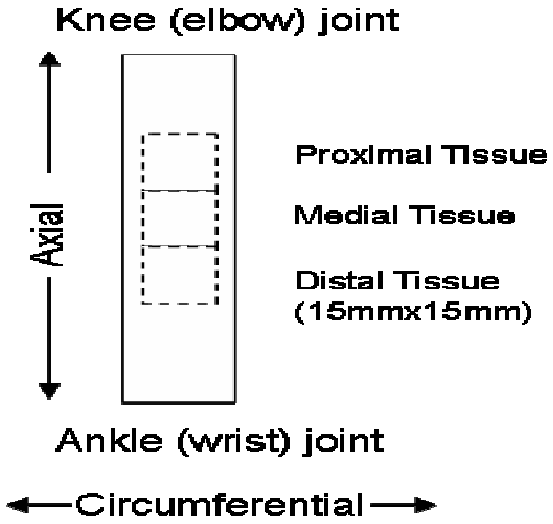

Figure 2.3 Tissues excised from bone and their general characteristics.

2.2.2 Mounting

A single piece of tissue was placed upon a dense, 15 x 15mm foam frame, cambium layer up, to facilitate the introduction of 12 hand-fabricated stainless steel hooks into the periphery of the tissue, 3 hooks per side (Figure 2.4).

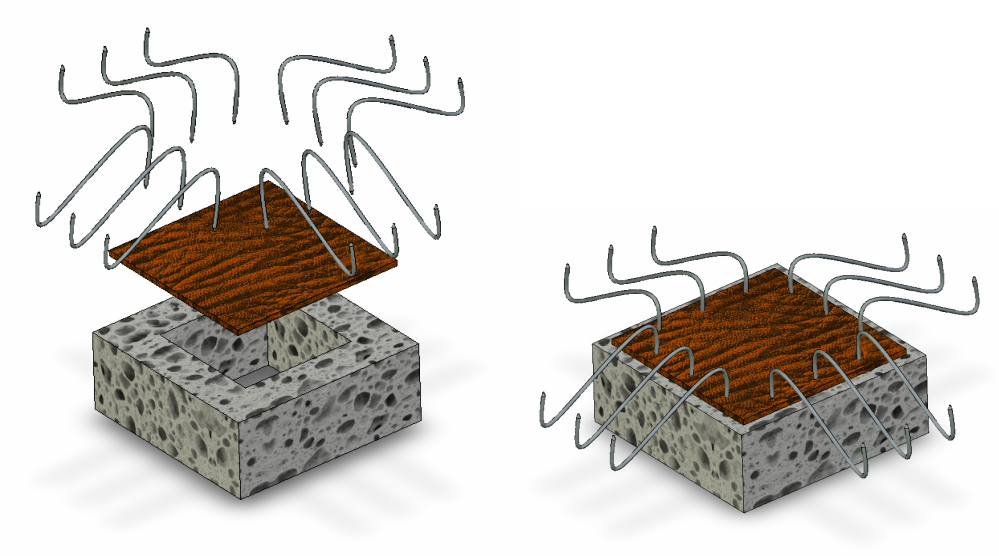

Figure 2.4 SolidWorks representation of exploded and assembled tissue with hooks.

The tissue/pad assembly was then placed into the center of the chamber, tissue side down, making sure the longitudinal direction of the tissue corresponded with the Y-axis of the chamber. The pre-strung sutures within the chamber were looped around the hooks, slight tension was applied, and the hooks were slowly worked out of the foam frame using forceps, taking care not to remove the hooks from the tissue. With the foam removed, room temperature saline was added until it contacted the tissue but did not cover it. Fascia was cleared away with the tissue stretched under a 30g load per side. Finally, four particles (G-850 Zeeospheres [3M]; approx. 100μm in diameter) were placed on the tissue approximately 1mm apart in a geometry attempting, but not necessitating, a square. Additional saline was then added until the tissue became immersed, and the markers were noted to stay in place.

2.3 Mechanical Tests

2.3.1 Mathematical Preliminaries

Our goal of qualitatively exploring the biaxial mechanical behavior of periosteum is facilitated by force-displacement data. Because there can be variations in the size of the region over which the forces are applied from tissue to tissue, it is more appropriate to compare in terms of stress-stretch or stress-strain calculations. Stretch ratios in the 'x' and 'y' directions are defined as $\Lambda_1 = \sqrt{F_{11}^2 + F_{21}^2}$ and $\Lambda_2 = \sqrt{F_{22}^2 + F_{12}^2}$, respectively, where F_{xx} are components of the 2D deformation tensor. While these calculations are used for our analyses, the simplified forms $\lambda_1 = F_{11}$ and $\lambda_2 = F_{22}$ are utilized in the feedback control due to the inability of our device to compensate for shearing. For this same reason, care is taken to ensure stretching of the tissue along or near its principal directions so that the off-diagonal terms remain small, and $\lambda_i \approx \Lambda_i$.

2.3.2 Protocols

Once mounted, the tissue was relaxed and the locations of the tracking markers recorded as reference configuration, β_R. The tissue was then stretched to its *in vivo* dimensions and a new configuration β_{IV} recorded. Next, the tissue was preconditioned from 2 to 80g biaxially for five cycles, and then relaxed to define a final reference configuration, β_P. Three types of tests were performed on each tissue - equibiaxial, constant stretch, and proportional. All tests were performed for five cycles, and stretches were calculated relative to β_P. For the equibiaxial test, the stretch ratios in each direction were maintained equal ($\lambda_1 = \lambda_2$) while the tissue was cycled between a

lower stretch ratio limit of 1.03 and an upper load limit of 100g. The maximum stretch ratio achieved was recorded as λ_{max}. The constant stretch tests called for maintaining one direction at $\lambda = \lambda_{max}$, while the other direction was cycled between stretch ratios of 1.03 and λ_{max}. The constant stretch test was repeated for the other direction. Finally, the proportional test maintained the stretch of the less-stiff direction at twice the stretch of the stiffer direction ($\lambda_{less\text{-}stiff} = 2\ \lambda_{stiff}$) while the tissue was cycled between a lower stretch ratio limit of 1.03 and an upper load limit of 100g. All tests were performed for five cycles at a stretch rate of approximately 0.14% per second, marker histories and forces were monitored at 30Hz, and the fifth cycle was used for analysis.

2.4 Data Processing

2.4.1 Pre-Analysis

A median filter was applied to the raw data, and the output was further reduced by selecting every 15th point. We assume the periosteum has negligible bending stiffness, experiences plane-stress, and that the stress does not vary through the thickness. Therefore we employ the membrane theory of continuum mechanics, and use the two dimensional forms of the Cauchy membrane stress **T**, shown below in Equation 1, and left stretch tensor **V**, shown below in Equation 2. P, Equation 3, represents the first Piola-Kirchoff stress comprised of forces, f, in the present configuration related to lengths in the reference configuration, L. F represents the 2-dimensional deformation tensor, Equation 4. **V** is more clearly defined by Equation 5.

$$\mathbf{T} = \frac{1}{\det(\mathbf{F})}\mathbf{F}\cdot\mathbf{P} \qquad (1)$$

$$\mathbf{V}^2 = \mathbf{B} \tag{2}$$

$$\mathbf{P} = \begin{bmatrix} \dfrac{f_x}{L_2} & 0 \\ 0 & \dfrac{f_y}{L_1} \end{bmatrix} \tag{3}$$

$$\mathbf{F} = \begin{bmatrix} \dfrac{\partial x_1}{\partial X_1} & \dfrac{\partial x_1}{\partial X_2} \\ \dfrac{\partial x_2}{\partial X_1} & \dfrac{\partial x_2}{\partial X_2} \end{bmatrix} \tag{4}$$

$$\mathbf{B} = \mathbf{F} \cdot \mathbf{F}^{\mathbf{T}} \tag{5}$$

Because the tissue is highly anisotropic (relative to β_P), data was compared in terms of tensor magnitudes, which condense the biaxial data to single scalar quantities. The magnitude of a general tensor A is

$$|\mathbf{A}| = \sqrt{tr\left(\mathbf{A} \cdot \mathbf{A}^{\mathbf{T}}\right)}\,. \tag{6}$$

Recall that we used tissues from pigs involved with other studies. As such, we could not control for parameters such as diet, age at sacrifice, daily routine, or gender. Furthermore, though all tissues were removed from the same humeral facet of each pig, removal from precisely the same anatomical coordinates is virtually impossible. Indeed, geometrical variations between ulna were observed even for pigs of similar size. For these reasons, we analyzed the mean mechanical responses across seven subgroups of tissues, grouped according to: pig number, left limb, right limb, proximal, medial, distal, and all tissues. For calculating the means, a linear interpolation function was utilized to find stretch values at specific values of membrane stress incremented by 0.5

N/m. For each increment of stress, the values of stretch were averaged. The various means were plotted against one another, with corresponding standard deviations.

2.4.2 Constitutive Modeling

Data from Equibiaxial, Constant-X, and Constant-Y tests for all tissues was pooled to create twenty data sets to fit each with an individual model. This process was done by finding the components of the Cauchy stress, which are easily calculated from data using the component form in Equation 7.

$$T_{ij} = \sum_{k=1}^{2} \frac{1}{\det(F)} F_{ik} \cdot P_{kj} \tag{7}$$

A Levenberg-Marquardt nonlinear least squares regression was then used in MATLAB to fit the calculated stresses to the general constitutive relation for a hyperelastic membrane, Equation 8.

$$T_{ij} = \sum_{k=1}^{2} \sum_{p=1}^{2} \frac{1}{\det(F)} F_{ik} F_{kp} \frac{\partial w}{\partial E_{pj}} \tag{8}$$

E_{pj} are the components of the 2D Green strain tensor, shown in Equation 9, where I denotes an identity tensor.

$$E_{pj} = \sum_{i=1}^{2} \frac{1}{2} \left(F_{ip} F_{ij} - I_{pj} \right) \tag{9}$$

Equation 10 is the chosen seven-parameter Fung-type 2D pseudo-strain energy function. It incorporates both Q, Equation 11, and c for the various seven coefficients.

$$w = c \exp(Q - 1) + \frac{1}{2}(c_4 E_{11}^2 + c_6 E_{22}^2) + c_5 E_{11} E_{22} \tag{10}$$

$$Q = \frac{1}{2}(c_1 E_{11}^2 + c_3 E_{22}^2) + c_2 E_{11} E_{22} \tag{11}$$

Convergence of this model and each set of data was satisfied when the error changed by less than 1E-07 in a single iteration. Each data set produced a group of 7 coefficients.

CHAPTER 3

RESULTS

Efficacy of our device to perform the stretch protocols herein was easily shown by graphically comparing the stretch ratios for each direction through a loading-unloading cycle (Figure 3.1). Control was well within acceptable tolerances, and was repeatable for all tests.

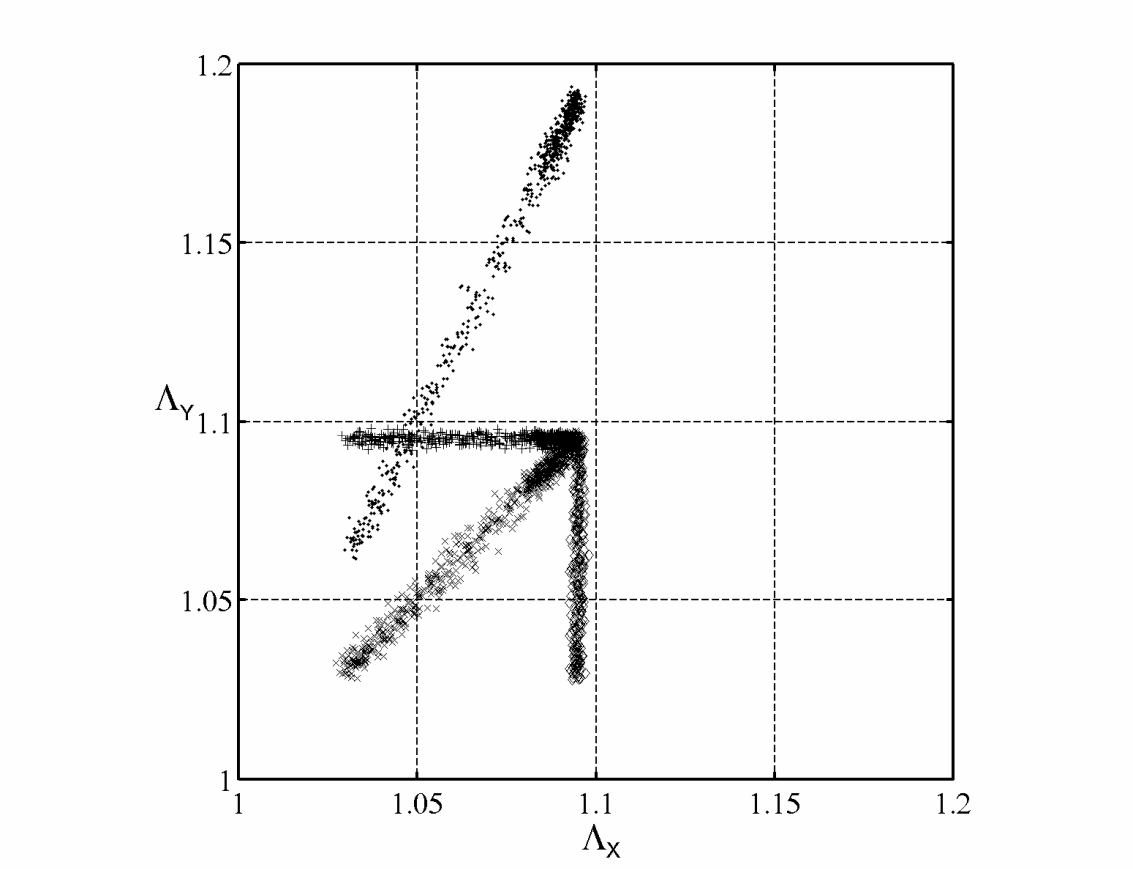

Figure 3.1 Four types of biaxial stretch protocols plotted as stretch ratio in x and y directions.

3.1 Mechanical Behavior

Equibiaxial stretching data are appropriate for evaluating general mechanical characteristics and material symmetry, and for revealing potential functional forms for constitutive relations. Similar to other collagenous membranes, the periosteum is anisotropic and transitions from an easily extensible state to a near inextensible state over a relatively short range of stretch (Figures 3.2 and 3.3a). Preconditioning affects (not shown) and hysteresis were almost negligible, which may be attributed to the low rate of stretch. The circumferential direction is clearly less extensible when tests were performed relative to the preconditioned configuration β_P. Recalculating the stretches relative to the *in vivo* configuration β_{IV}, however, suggests the axial direction is the least extensible when the tissue is attached to the bone (Figure 3.3b). This discrepancy is primarily attributed to anisotropic tissue contraction (shrinkage) when removed from the bone, which is more pronounced in the axial direction (Figures 3.3b and 3.4). Finally, the proportional stretch tests reveal an interesting interplay between the stretching axes. That is, the amount of stretch in the less-stiff direction has little or no effect on the stress in the stiffer direction within the tested range (compare Figures 3.3a and 3.3c).

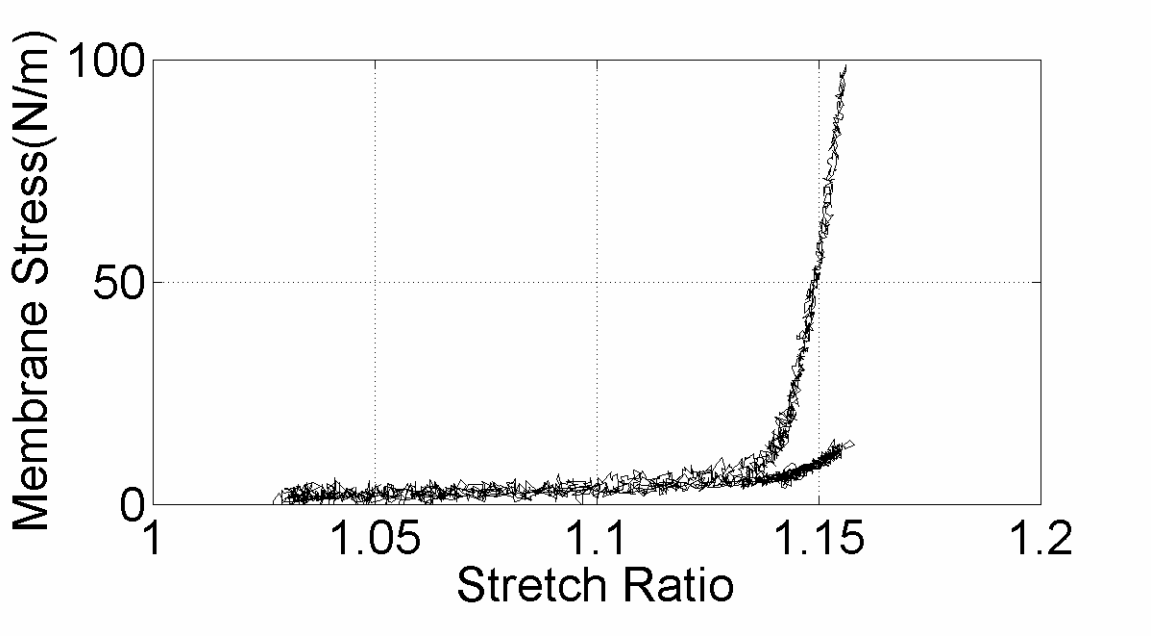

Figure 3.2 Representative raw biaxial data from loading and unloading during an equibiaxial test on porcine periosteum. The line reaching greater stress represents the circumferential direction, while the less-stiff line represents the axial direction. The lack of smoothness is not due to the bi-directionality of the data but the sensitivity of the equipment in use.

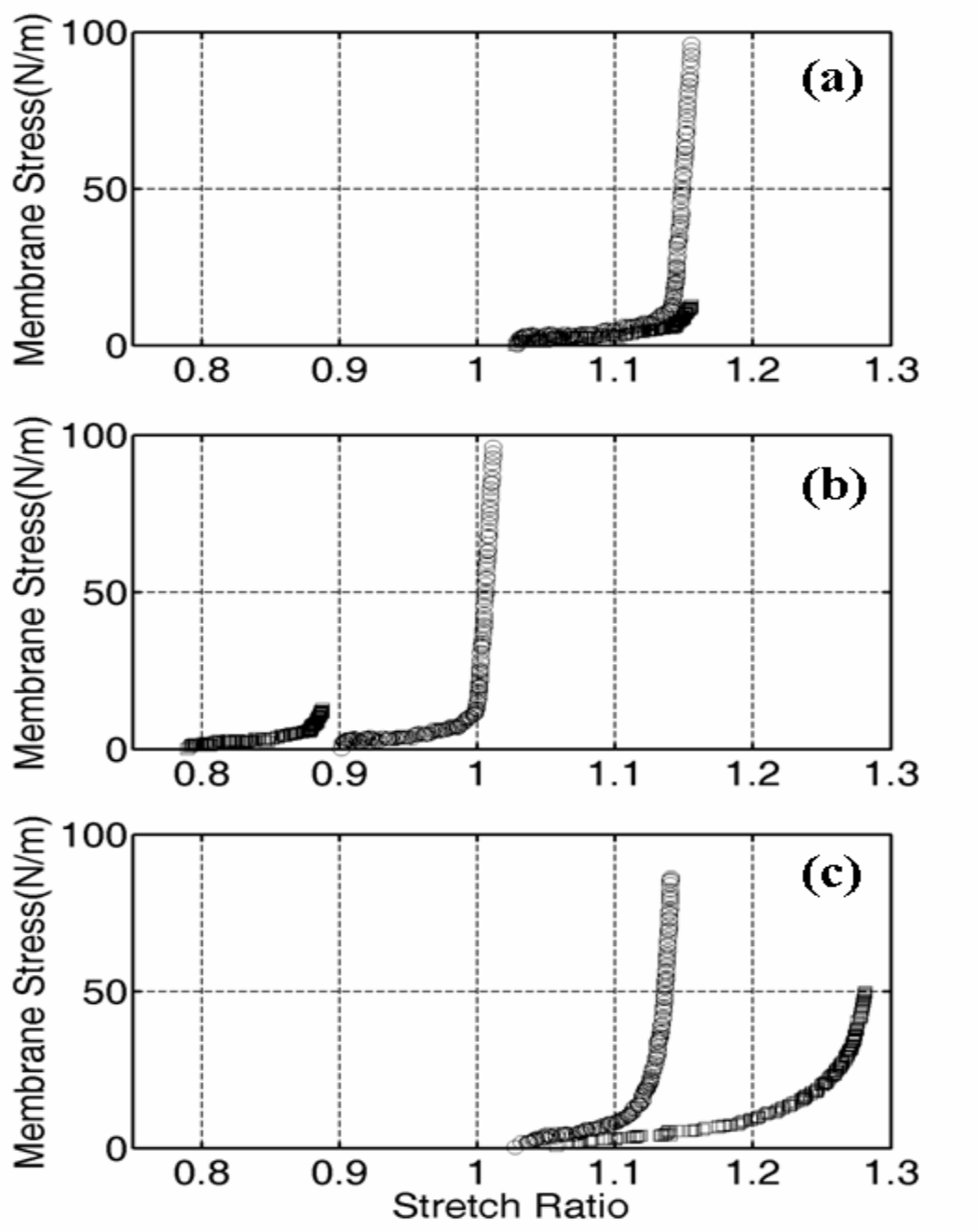

Figure 3.3 Representative reduced data for (a) Equibiaxial with stretches calculated relative to β_P, (b) Equibiaxial stretches relative to β_{IV} and (c) Proportional data relative to β_P. Comparison of (a) and (b) reveals effect of different reference configurations, while comparisons of (a) and (c) reveal the indifference of the circumferential stress to the axial stretch within the range of stretches tested. Circumferential (o) and Axial (□).

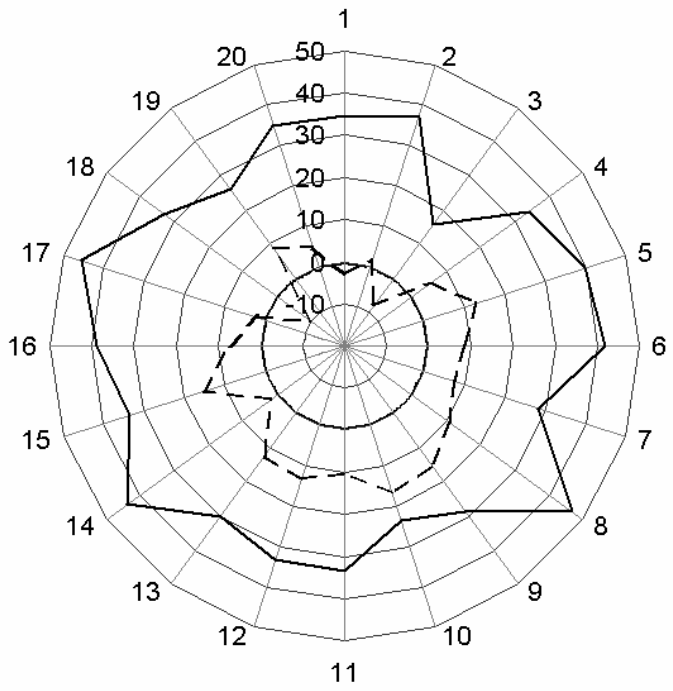

Figure 3.4 Tissue shrinkage as a percentage decrease from *in vivo* size for all twenty tissues corresponding with values found in Table 3.2. Negative values indicate an increase in size. Darker circle represents zero percent. Circumferential (Dashed) and Axial (Solid).

3.2 Histology

Structural features that may give rise to the observed shrinkage and mechanical behavior were observed histologically. Transverse sections taken along the axial and circumferential directions reveal three distinct layers – an inner cellular layer (cambium), an intermediate layer of small and compact collagen fibers interwoven with elastin, and an outer layer of larger collagen fibers (Figures 3.5 and 3.6). Collagen and elastin fibers in the intermediate layer are crimped and oriented along the axis of the bone. The larger collagen fibers of the outer layer travel in the circumferential

direction, and are more mildly crimped. The relatively large quantity of elastin in the axial direction coincides well with the higher degree of shrinkage in that direction. Similarly, the lower degree of undulation and lack of elastin in the outer layer correlates well with the lesser degree of shrinkage in the circumferential direction (Figure 3.4).

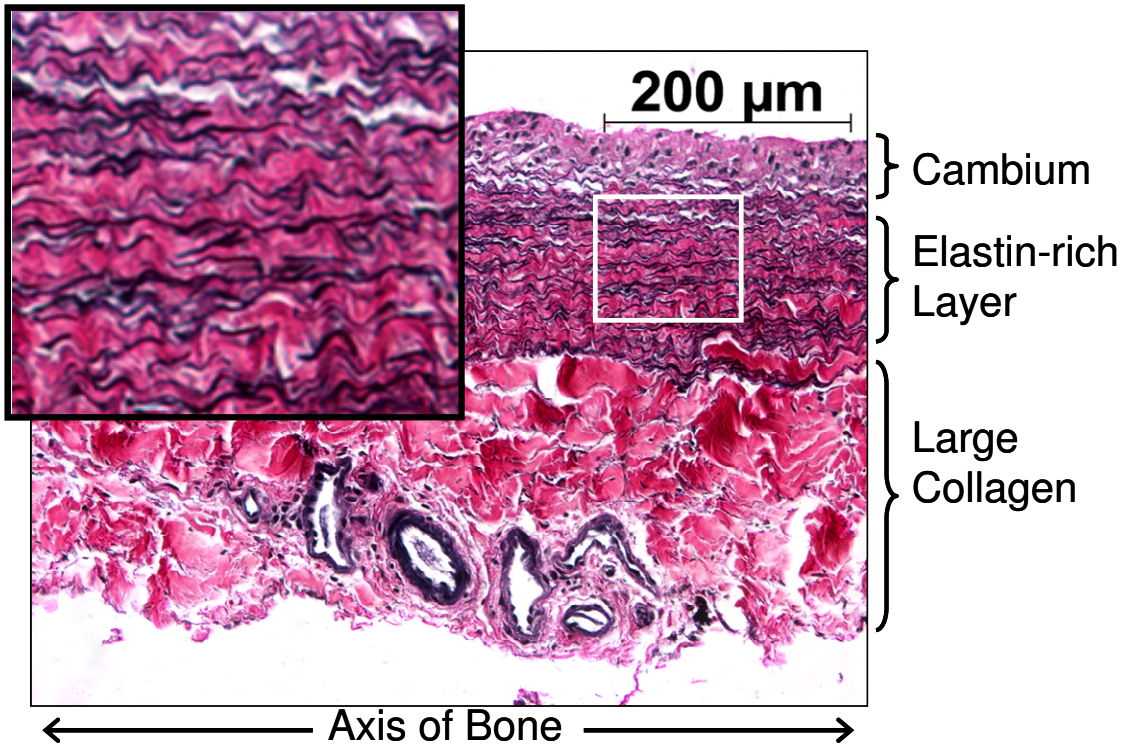

Figure 3.5 Axial section of periosteum demonstrating orientation of elastin fibers along long axis of bone, and marked division in tissue (Weigert's H&E 20X). Inset is close-up of boxed region.

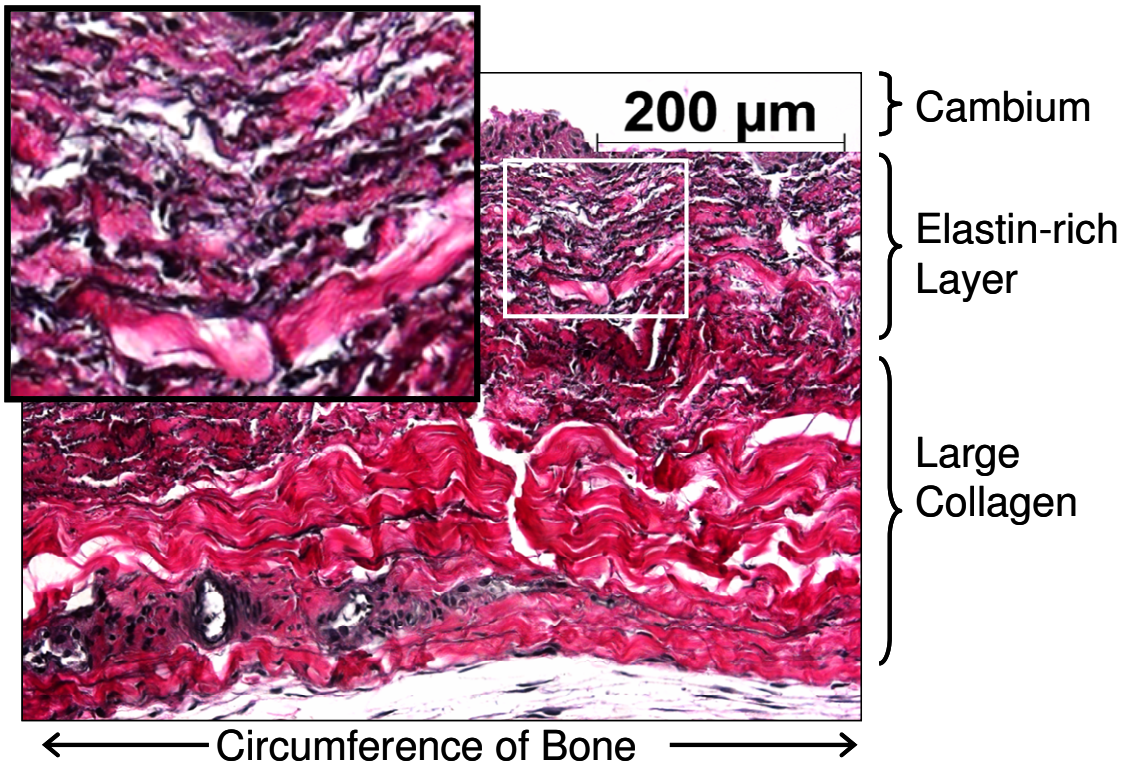

Figure 3.6 Circumferential section of periosteum demonstrating the orientation of the undulating collagen fibers around the bone circumference and the apparent cleavage of elastin fibers running axially (Weigert's H&E 20X). Inset is close-up of boxed region.

3.3 Inter- and Intra-pig variability

Mean mechanical responses from the nine subgroups of pigs – pig number (1 to 4), left limb, right limb, proximal, medial, and distal tissues – are compared in Figures 3.7 through 3.9. Recall that comparisons were made on the basis of tensor magnitudes to better account for mild differences in material symmetry. For reference, the special case wherein the tissue is unstretched (i.e. $\lambda_x = \lambda_y = 1$) corresponds to a stretch magnitude $|V|$ of approximately 1.41.

Inter-pig variability was more pronounced than intra-pig variability, but no statistically significant variations in |V| at a specific value of |T| were observed within any of the comparison groups (Figures 3.7 – 3.9). General mechanical characteristics were similar across all pigs and anatomical locations tested. On average, tissues transitioned from an easily extensible state to a near inextensible state near |V| = 1.63, which corresponds to an equibiaxial stretch of $\lambda_x = \lambda_y \approx 1.15$.

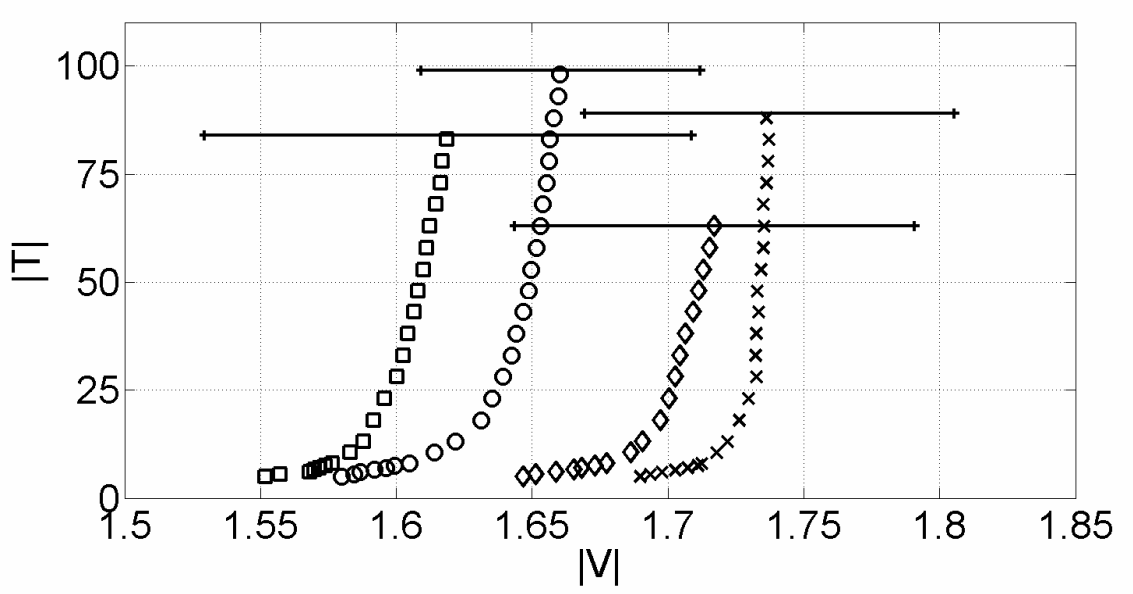

Figure 3.7 Mean mechanical response for Pigs 1 (◊, n=4), 2 (×, n=4), 3 (o, n=6), and 4 (□, n=6) plotted as magnitude of Cauchy membrane stress vs. magnitude of left stretch tensor. Bars represent one standard deviation.

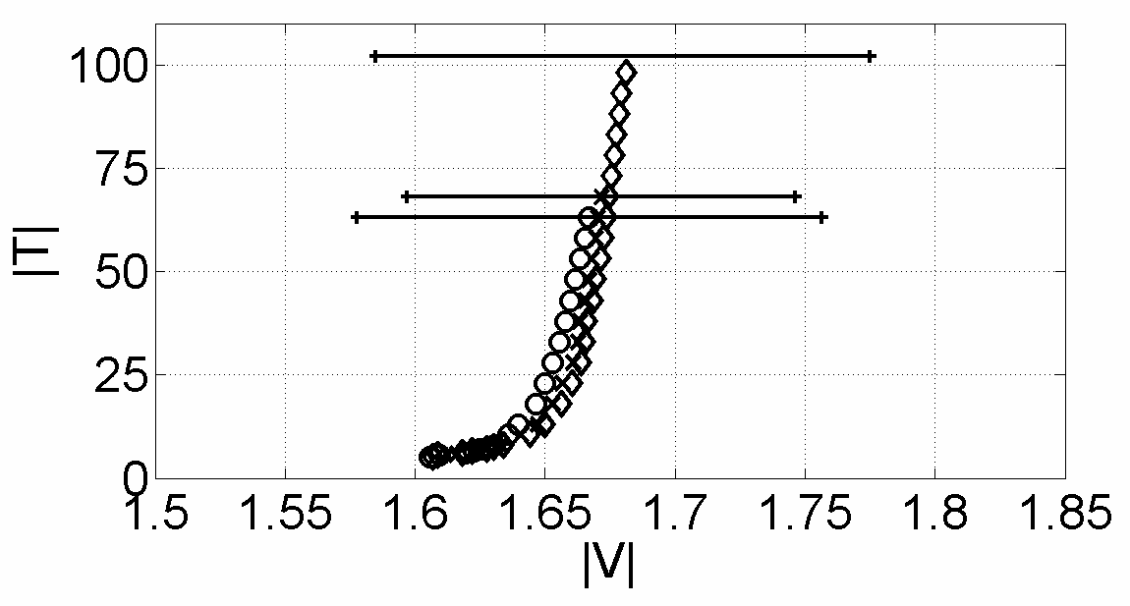

Figure 3.8 Mean mechanical response for locations Proximal (◊, n=6), Medial (×, n=7), and Distal (o, n=7) plotted as magnitude of Cauchy membrane stress vs. magnitude of left stretch tensor. Bars represent one standard deviation.

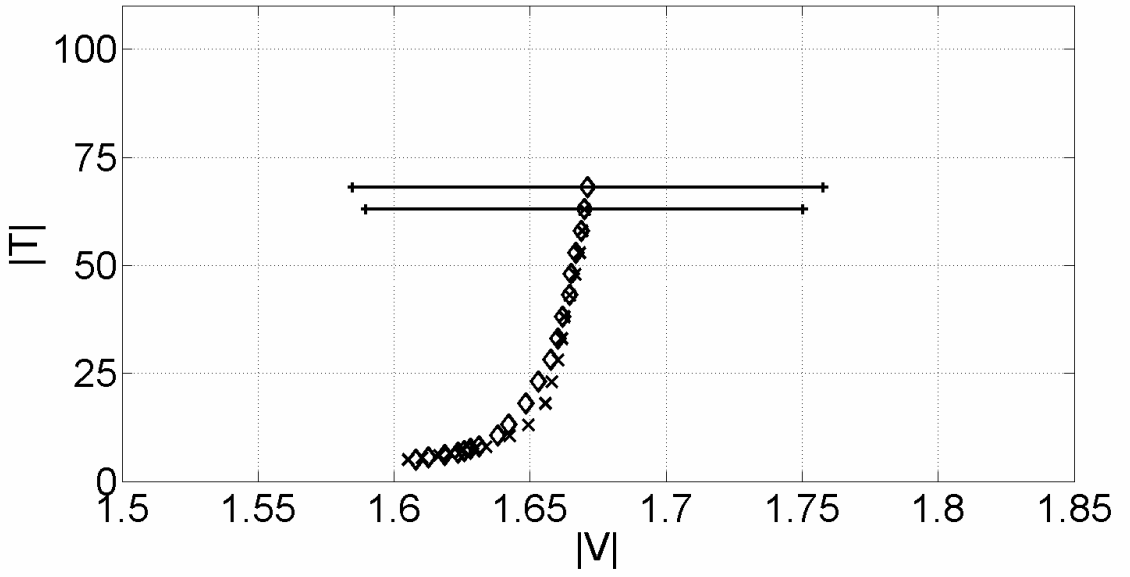

Figure 3.9 Mean mechanical response for Left (◊, n=11) and Right (×, n=9) plotted as magnitude of Cauchy membrane stress vs. magnitude of left stretch tensor. Bars represent one standard deviation.

Table 3.1 identifies the mean values for the tissue shrinkage and mean mechanical response data. Z-tests were performed to identify statistical similarity between the means of the data sets. All the means compared generated Z-values that would indicate similarity at α=0.01, except for the circumferential and axial comparison, which has statistically dissimilar means.

Table 3.1 Statistical comparison of data sets using $2.58 \geq Z \geq -2.58$ to represent statistical similarity at α=0.01.

Tissue Characteristic	Mean	Standard Deviation	Statistical Comparison	Z-value	α=0.01 Means are:
Circumferential	6.50	7.50	Circ.-Axial	-11.49	Different
Axial	33.97	7.63			
			Pig1-Pig2	-1.61	Similar
Pig 1	1.668	0.050	Pig1-Pig3	0.25	Similar
Pig 2	1.736	0.069	Pig1-Pig4	1.11	Similar
Pig 3	1.660	0.051	Pig2-Pig3	1.90	Similar
Pig 4	1.619	0.090	Pig2-Pig4	2.34	Similar
			Pig3-Pig4	0.97	Similar
Proximal	1.662	0.072			
Medial	1.664	0.072	Proximal-Medial	-0.05	Similar
Distal	1.661	0.092	Proximal-Distal	0.02	Similar
			Medial-Distal	0.07	Similar
Left	1.663	0.087			
Right	1.657	0.062	Left-Right	0.18	Similar

3.4 Constitutive Modeling

Recall that data from the equibiaxial, constant-x, and constant-y tests were simultaneously fit using a single regression for each tissue, yielding a unique set of coefficients for each tissue (Table 3.2). The seven-parameter Fung-type constitutive model fit the tissue data well (Figure 3.10). Because of the high variance of parameters from tissue to tissue, however, predicting mechanical behavior of an untested tissue

with this model is unlikely. Furthermore, the model performed poorly in predicting the stresses for the proportional loading protocol on the same tissue (Figure 3.11).

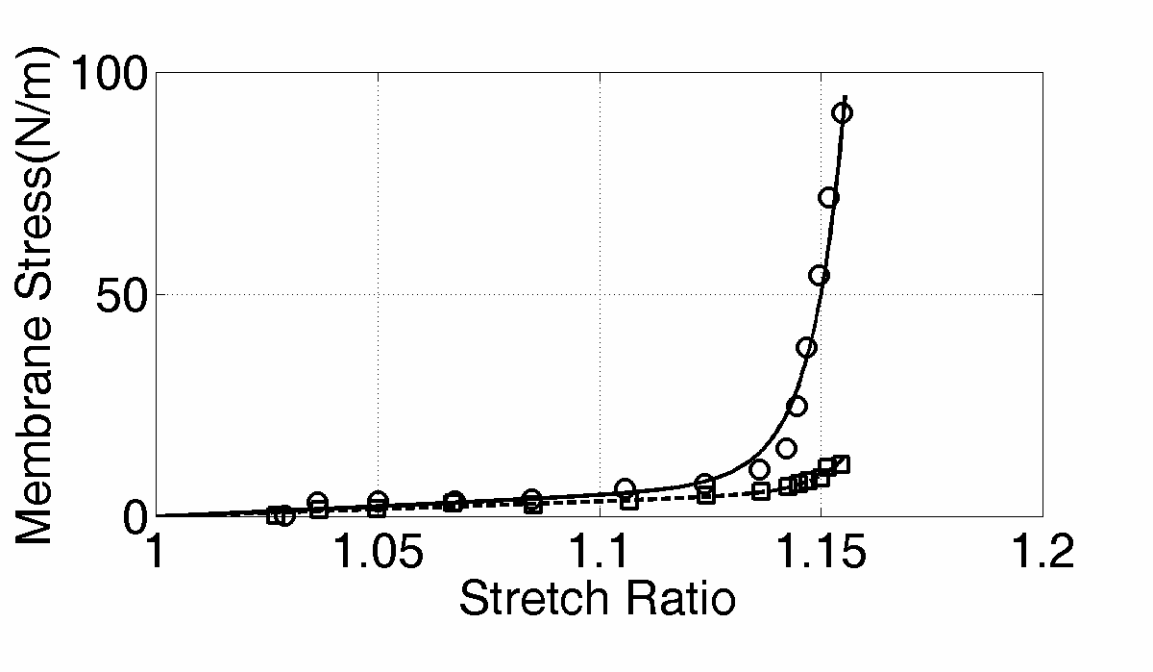

Figure 3.10 Representative fit of Equation 8 to equibiaxial data. Circumferential (Solid vs. o) and Axial (Dashed vs. □).

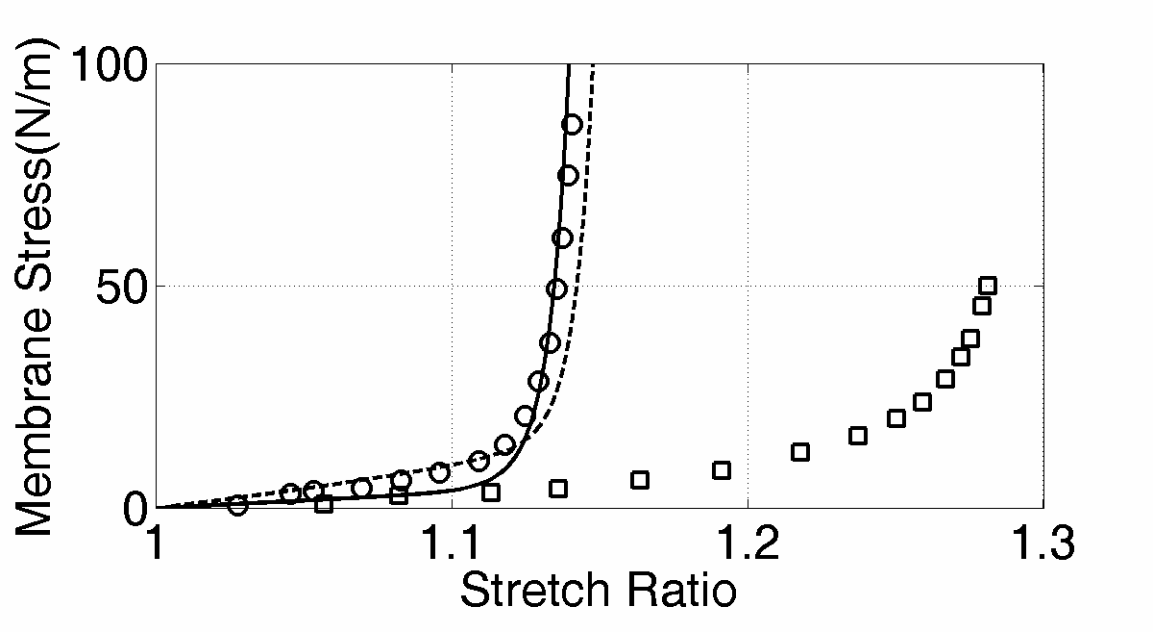

Figure 3.11 Representative prediction of mechanical behavior during a proportional test using parameters determined with the Equibiaxial, Constant-X, and Constant-Y data. The model fails to adequately fit the axial direction. Circumferential (Solid vs. o) and Axial (Dashed vs. □).

Table 3.2 General and coefficient information organized for each tissue.

Pig	Tissue	Limb	Location	c (N/m)	c1	c2	c3	c4 (N/m)	c5 (N/m)	c6 (N/m)
1	1	Left	Distal	*0*	*791.5447*	*61.1345*	*40.9451*	*26.3509*	*0.0004*	*18.9909*
	2	Left	Medial	*0.0001*	*453.9238*	*0*	*0*	*11.2629*	*0*	*0.0521*
	3	Right	Distal	*0.0001*	*353.7960*	*11.4042*	*0*	*16.9391*	*21.3145*	*0*
	4	Right	Proximal	*0*	*391.8265*	*27.4744*	*3.3250*	*20.0692*	*15.0441*	*0.0252*
2	5	Right	Medial	*0.0007*	*452.9158*	*0*	*0*	*0*	*0*	*7.0518*
	6	Left	Proximal	*0.0018*	*526.1451*	*0*	*0*	*0*	*0*	*0*
	7	Left	Medial	*0*	*460.3452*	*61.3329*	*29.6954*	*0.3329*	*0.3783*	*20.9814*
	8	Left	Distal	*0*	*461.9797*	*0*	*19.5730*	*37.9948*	*0*	*2.7559*
3	9	Right	Proximal	*0.0001*	*586.3037*	*0*	*54.1370*	*35.1797*	*0*	*39.8909*
	10	Right	Medial	*0*	*632.3932*	*0*	*34.8923*	*40.8809*	*0*	*32.6026*
	11	Right	Distal	*0.0114*	*575.5121*	*45.1443*	*0*	*0*	*0*	*0*
	12	Left	Proximal	*0.0012*	*446.7328*	*0*	*16.5093*	*3.7279*	*0*	*33.9733*
	13	Left	Medial	*0.0027*	*470.8768*	*18.9652*	*15.0815*	*48.7771*	*0*	*24.7694*
	14	Left	Distal	*0.0082*	*699.4747*	*3.9407*	*0*	*0*	*0*	*0*
4	15	Right	Proximal	*0*	*385.1879*	*11.8596*	*14.8101*	*0*	*26.5580*	*9.7695*
	16	Right	Medial	*0.0094*	*893.1671*	*0*	*0*	*0*	*0*	*0*
	17	Right	Distal	*0.0025*	*1150.8561*	*46.8720*	*0*	*0*	*0*	*0*
	18	Left	Proximal	*0.0007*	*2209.9499*	*60.7868*	*0*	*0*	*0*	*0*
	19	Left	Medial	*0.0196*	*550.8204*	*32.9640*	*1.5731*	*5.6094*	*0*	*45.4447*
	20	Left	Distal	*0.0014*	*311.5373*	*0.4247*	*31.8224*	*27.7867*	*0*	*28.0690*
			Average	0.0030	640.2644	19.1152	13.1182	13.7456	3.1648	13.2188
			St Dev	0.0052	420.5381	23.6298	16.8484	16.6723	7.9000	15.7846

CHAPTER 4

DISCUSSION

The periosteum is a key contributor of osteoprogenitor cells during bone growth and adaptation, trauma repair, and callotasis [Kojimoto et al., 1988]. The processes that call these cells into action are not understood fully, but it is generally accepted that mechanical loading plays a significant role by instigating recruitment, proliferation, and/or differentiation of the periosteal cells. Mechanical characterization of the periosteum, therefore, is a prudent step in deciphering these roles. Because the periosteum is three-dimensional and likely subjected to multiaxial loads *in vivo*, simple uniaxial tests are insufficient for a full mechanical characterization. Herein, we've made use of the membrane theory in continuum mechanics to reduce periosteal mechanics to a two dimensional problem, and we've presented the first biaxial interrogation of periosteal mechanics.

4.1 General Mechanical Characteristics

Reports on periosteal microstructure reveal both a species and location dependence, making direct comparisons to previous studies a challenge. The porcine periosteum herein has at least three distinct layers – a cellular layer, an elastin-rich layer, and a collagen-rich layer – the latter two providing structural integrity. Not surprisingly then, the general biaxial mechanical characteristics of periosteum resemble those of other collagen and/or elastin-rich membranes [Vawter et al., 1978; Lanir, 1979;

Kang et al., 1996; Chew et al., 1986; Billiar and Sacks, 2000]. Collagen is the stretch-limiting constituent, becoming near-inextensible when pulled taut, and therefore dominates in the steep region of the stress-stretch plot. Conversely, elastin plays the more significant role in lower ranges of stretch, giving rise to the mild slope in the initial region of the stress-stretch plot [Kang et al., 1996]. The transition, or elbow, region represents the sequential recruitment of collagen fibers as they become fully stretched (uncrimped). Anisotropy is marked, likely because of the sharp delineation between the two orthogonally-opposed fibrous layers with primary fiber directions corresponding to the axes of stretch. Collagen bands of the collagen-rich layer run in the circumferential direction, have fewer periodic undulations, and appear thicker when compared to the fibers of the elastin-rich layer that are oriented along the bone axis. Thus giving rise to the higher apparent stiffness in the circumferential direction.

4.2 *In Vivo* Condition

Notably, tissue shrinkage was significantly more pronounced in the axial direction when removed from the bone, corresponding well to the dense population of elastin fibers oriented in that direction. Hence, the stiffer direction *in situ* can not be inferred directly from our tests. Indeed, Figure 3.3 shows plainly that, while the circumferential direction was stretched to its *in vivo* length ($\lambda^* = 1$) during our equibiaxial tests, the axial direction remained far below its *in vivo* length. Based on this result, and our observations that loads of greater than 60g (~ 40 N/m) in each direction were required to hold the tissue at its *in vivo* dimensions (not reported), we surmise that the tissue exists in a highly stressed state when attached to the bone.

4.2.1 Other Findings

This correlates well to the findings of several investigators who have shown increased longitudinal growth when the periosteum is "released" through circumferential incision, due to its proposed role as a mechanical restraint to growth [Wilson-MacDonald et al., 1990; Crilly, 1972; Warrell and Taylor, 1979; Harkness and Trotter, 1978; Lynch and Taylor, 1987]. Our findings are contrary, however, to the observations of Bertram et al. (1998), who suggest that periosteum is only mildly stressed *in vivo* and therefore cannot mechanically constrain longitudinal growth. The discrepancy in observations is likely due to the uniaxial nature of their tests. Briefly, they fixed both ends of an avian long-bone in a uniaxial stretching fixture, placed two lines on the periosteum to demarcate the *in vivo* length, and then cleverly removed the diaphyseal region of the bone while preserving an intact strip of periosteum connected to the two bone ends. Then they performed a single full-range stretching test to failure while monitoring the force and displacement between the two lines. The stress at the original length was easily determined from the data. However, it is probable that the tissue relaxed in the circumferential direction when they removed the diaphysis of the bone, as there were no constraints preventing it from doing so. This would have reduced the level of stress and increased the tissue length in the axial (longitudinal) direction, thereby underestimating the true *in vivo* longitudinal stress.

4.3 Tissue Variability

Variability in mechanics from one tissue to the next is typical, and may be due to differences in tissue constituents, microstructure, and/or geometry. This confounds

rigorous quantitative analyses on how periosteal mechanics change when, for example, subjected to supraphysiologic loads during callotasis. Enlightening qualitative analyses are possible, however, provided the inter-tissue variability is reasonably small or distributed fairly even about some mean. Clearly, the mean mechanical responses for the four pigs are qualitatively similar, but span a wide range of stretches. Still, the differences are statistically insignificant for any two pigs, and they are well distributed about the overall mean. Differences between the means were all but negated when we grouped the tissues according to location (proximal, medial, or distal) and limb (left or right). Thus, our data suggest one may somewhat indiscriminately pool periosteal samples from multiple pigs and multiple locations, within the limits tested herein, for a common parametric analysis.

4.4 Constitutive Modeling

Ultimately, an understanding of periosteal mechanics may prove most beneficial when incorporated into computational bone growth models. As such, a relevant constitutive relation must be identified and the material parameters determined. Herein, we chose only to investigate the utility of an existing relation, which has modeled well other collagenous tissues (eg. endocardium [Kang et al., 1996]). The model fit the data well for both axes, but material parameters varied widely between tissues. Common for all tissues, however, was the dominance of the exponential parameter associated with E11, the strain in the circumferential direction. This appears to agree with the observed indifference of the circumferential stress to the axial stretch within the range of stretches tested (compare the circumferential plots in Figures 3.3a and 3.3c). This

dominance is likely responsible also for the poor fit to the proportional data (Figure 3.11). In essence, the model is relatively insensitive to the increased axial stretch and is probably not suited well to predicting the mechanical stress of this tissue for any non-equibiaxial deformation. A better constitutive model is needed.

The model used herein incorporates a single pseudo-strain energy function applied to a complex, multi-constituent tissue. Alternatively, one may use a slightly more sophisticated model that accounts better for the observed ultrastructure (i.e. a microstructural model). For example, the two distinct structural layers can be modeled as independent membranes stretched in parallel. The stress in each membrane could then be described in terms of separate pseudo-strain energy functions (according to Equation 7) with unique sets of coefficients, then summed. As suggested in Kang et al. (1996), perhaps a seven-parameter model would work best for the elastin-rich layer while a simpler four-parameter model may work for the collagen-rich layer. Of course, such a model assumes the unlikely scenario that the two structural layers act independently of one another. Still, investigation of such models is worthwhile and will be a focus of our future work.

4.5 Future Work

As a preliminary analysis, there is much future work that can strengthen and build upon our findings and those of others. Evaluating the alterations in mechanical behavior for periosteum cultured under well-controlled boundary conditions is a planned follow-up to this work, and may help elucidate the effects of callotasis on periosteum. Further mechanical testing and/or microstructural analysis may help

elucidate the physical relationship between the principal stretching axes. Ultimately, a modeling approach that incorporates both phenomenological and microstructural arguments may yield the optimal constitutive relation.

REFERENCES

Agata H, Asahina I, Yamazaki Y, Uchida M, Shinohara Y, Honda MJ, Kagami H, Ueda M (2007) Effective Bone Engineering with Periosteum-derived Cells. J Dent Res 86: 79-83.

Allen MR, Hock JM, Burr DB (2004) Periosteum: biology, regulation, and response to osteoporosis therapies. Bone 35: 1003-1012.

Balena R, Shih M, Parfitt AM (1992) Bone Resorption and Formation on the Periosteal Envelope of the Ilium: A Histomorphometric Study in Healthy Women. J Bone Min Res 7: 1475-1482.

Bertram JEA, Polevoy Y, Cullinane DM (1998) Mechanics of Avian Fibrous Periosteum: Tensile and Adhesion Properties During Growth. Bone 22: 669-675.

Brighton CT, Lorich DG, Kupcha R, Reilly TM, Jones AR, Woodbury II RA (1992) The Pericyte as a Possible Osteoblast Progenitor Cell. Clin Orthop Rel Res 275: 287-299.

Carpenter RD, Carter DR (2007) The mechanobiological effects of periosteal surface loads. Biomech Model Mechanobiol May 9 [Epub ahead of print].

Carter DR, Beaupre GS, Giori NJ, Helms JA (1998) Mechanobiology of Skeletal Regeneration. Clin Orthop Rel Res 355: 41-55.

Chenu C, Colucci S, Grano M, Zigrino P, Barattolo R, Zambonin G, Baldini N, Vergnaud P, Delmas PD, Zallone AZ (1994) Osteocalcin Induces Chemotaxis, Secretion of Matrix Proteins, and Calcium-mediated Intracellular Signaling in Human Osteoclast-like Cells. J Cell Bio 127: 1149-1158.

Cowin SC (2001) Bone Mechanics Handbook 2nd Ed. CRC Press, Boca Raton.

De Bastiani G, Aldegheri R, Renzi-Brivio L, Trivella G (1987) Limb lengthening by callus distraction (callotasis). J Pediatr Orthop 7(2): 129-34.

Downs J, Halperin HR, Humphrey JD, Yin F (1990) An Improved Video-Based Computer Tracking System for Soft Biomaterials Testing. IEEE Transactions on Biomedical Engineering 37: 903-907.

Einhorn TA (1998) The Cell and Molecular Biology of Fracture Healing. Clin Orthop Rel Res 355: 7-21.

Ellender G, Feik SA, Ramm-Anderson SM (1989) Periosteal changes in mechanically stressed rat caudal vertebrae. J Anat 163: 83-96.

Epker BN, Frost HM (1966) Periosteal Appositional Bone Growth from Age Two to Age Seventy in Man: A Tetracycline Evaluation. Anat Rec 154: 573-578.

Hankenson KD, Ausk BJ, Bain SD, Bornstein P, Gross TS, Srinivasan S (2006) Mice lacking thrombospondin 2 show an atypical pattern of endocortical and periosteal bone formation in response to mechanical loading. Bone 38: 310-316.

Harris SE, Bonewald LF, Harris MA, Sabatini M, Dallas S, Feng JQ, Ghosh-Choudhury N, Wozney J, Mundy GR (1994) Effects of Transforming Growth Factor ß on Bone Nodule Formation and Expression of Bone Morphogenetic Protein 2, Osteocalcin, Osteopontin, Alkaline Phosphatase, and Type I Collagen mRNA in Long-Term Cultures of Fetal Rat Calvarial Osteoblasts. J Bone Min Res 9: 855-863.

Henderson JH, Carter DR (2002) Mechanical Induction in Limb Morphogenesis: The Role of Growth-generated Strains and Pressures. Bone 31: 645-653.

Herring JA (2002) Tachdjian's Pediatric Orthopaedics. W. B. Sauders Co, Philadelphia.
Horiuchi K, Amizuka N, Takeshita S, Takamatsu H, Katsuura M, Ozawa H, Toyama Y, Bonewald LF, Kudo A (1999) Identification and Characterization of a Novel Protein, Periostin, with Restricted Expression to Periosteum and Periodontal Ligament and Increased Expression by Transforming Growth Factor ß. J Bone Min Res 14: 1239-1249.

Hoshi K, Kemmotsu S, Takeuchi Y, Amizuka N, Ozawa H (1999) The Primary Calcification in Bones Follows Removal of Decorin and Fusion of Collagen Fibrils. J Bone Min Res 14: 273-280.

Hughes SS, Hicks DG, O'Keefe RJ, Hurwitz SR, Crabb ID, Krasinkas AM, Loveys L, Puzas JE, Rosier RN (1995) Shared Phenotypic Expression of Osteoblasts and Chondrocytes in Fracture Callus. J Bone Min Res 10: 533-544.

Humphrey JD, Vawter DL, Vito RP (1986) Quantifications of Strains in Biaxially Tested Soft Tissues. J Biomech 20: 59-65.

Humphrey JD, Wells PB, Baek S, Lai A, McLeroy, K, Yeh AT (2007) A theoretically-motivated biaxial tissue culture system with intravital microscopy. Biomech Model Mechanobiol Aug 14 [Epub ahead of print].

Ignatius A, Blessing H, Liedert A, Schmidt C, Neidlinger-Wilke C, Kaspar D, Friemert B, Claes L (2005) Tissue engineering of bone: effects of mechanical strain on osteoblastic cells in type I collagen matrices. Biomaterials 26: 311-318.

Jones DB, Nolte H, Scholubbers JG, Turner E, Veltel D (1991) Biochemical signal transduction of mechanical strain in osteoblast-like cells. Biomaterials 12: 101-110.

Kessler P, Bumiller L, Schlegel A, Birkholz T, Neukam FW, Wiltfang J (2007) Dynamic periosteal elevation. B J Oral Maxillofac Surg 45: 284-287.

Kuroda S, Virdi AS, Dai Y, Shott S, Summer DR (2005) Patterns and Localization of Gene Expression During Intramembranous Bone Regeneration in the Rat Femoral Marrow Ablation Model. Calcif Tissue Int 77: 212-225.

Lieberman JR, Daluiski A, Einhorn TA (2002) The Role of Growth Factors in the Repair of Bone. J Bone Joint Surg 84: 1032-1044.

Malizos KN, Papatheodorou LK (2005) The healing of the periosteum Molecular aspects. Injury, Int J Care Injured 36S: S13-S19.

Matziolis G, Tuisher J, Kaspar G, Thompson M, Bartmeyer B, Krocker D, Perka C, Duda G (2006) Simulation of Cell Differentiation in Fracture Healing: Mechanically Loaded Composite Scaffolds in a Novel Bioreactor System. Tissue Eng 12: 201-208.

Meyer MH, Meyer Jr RA (2007) Genes with Greater Up-Regulation in the Fracture Callus of Older Rats with Delayed Healing. J Orthop Res 25: 488-494.

Noonan KJ, Leyes M, Forriol F, Cañadell J (1998) Distraction Osteogenesis of the Lower Extremity with Use of Monolateral External Fixation. J Bone Joint Surg Am 80(6): 793-806.

O'Driscoll S, Saris D, Ito Y, Fitzsimmons J (2001) The chondrogenic potential of periosteum decreases with age. J Orthop Res 19: 95-103.

O'Driscoll SW, Meisami B, Miura Y, Fitzsimmons J (1999) Viability of Periosteal Tissue Obtained Postmortem. Cell Transpl 8: 611-616.

Orwoll ES (2003) Perspective: Toward an Expanded Understanding of the Role of the Periosteum in Skeletal Health. J Bone Min Res 18: 949-954.

Paley D, Catagni M, Argnani F, Prevot J, Bell D, Armstrong P (1992) Treatment of Congential Pseudoarthrosis of the Tibia Using the Ilizarov Technique. Clin Orthop Rel Res 280: 81-93.

Parfitt AM (1994) Special Article: The Two Faces of Growth: Benefits and Risks to Bone Integrity. Osteop Int 4: 382-398.

Pead MJ, Skerry TM, Lanyon LE (1988) Direct Transformation from Quiescence to Bone Formation in the Adult Periosteum Following a Single Brief Period of Bone Loading. J Bone Min Res 3: 647-656.

Popwics TE, Zhu Z, Herring SW (2002) Mechanical properties of the periosteum in the pig, *Sus scrofa*. Arch Oral Biol 47: 733-741.

Price JS, Oyajobi BO, Russell RGG (1994) The Cell Biology of Bone Growth. Eur J Clin Nutr 48: 131-149.

Raab-Cullen DM, Thiede MA, Peterson DN, Kimmel DB, Recker RR (1994) Mechanical Loading Stimulates Rapid Changes in Periosteal Gene Expression. Calcif Tissue Int 55: 473-478.

Radomsky ML, Thompson AY, Spiro RC, Poser JW (1998) Potential Role of Fibroblast Growth Factor in Enhancement of Fracture Healing. Clin Orthop Rel Res 355: 283-293.

Raisz LG (1984) Studies on Bone Formation and Resorption in vitro. Hormone Res 20: 22-27.

Ringe J, Kaps C, Burmester G, Sittinger M (2002) Stem cells for regenerative medicine: advances in the engineering of tissues and organs. Naturwissenschaften 89: 338-351.

Rios H, Koushik SV, Wang H, Wang J, Zhou H, Lindsley A, Rogers R, Chen Z, Maeda M, Kruzynska-Frejtag A, Feng JQ, Conway SJ (2005) *perostin* Null Mice Exhibit Dwarfism, Incisor Enamel Defects, and an Early-Onset Periodontal Disease-Like Phenotype. Molecular and Cellular Biol 25: 11131-11144.

Robins SP (1994) Biochemical markers for assessing skeletal growth. Eur J Clin Nutr 48: 199-209.

Sakata Y, Ueno T, Kagawa T, Kanou M, Fujii T, Yamachika E, Sugahara T (2006) Osteogenic potential of cultured human periosteum-derived cells- A pilot study of human cell transplantation into rat calvarial defect model. J Cran-Maxillofac Surg 34: 461-465.

Seeman E (2003) Periosteal Bone Formation- A Neglected Determinant of Bone Strength. N Engl J Med349: 320-323.

Seeman E (2007) The periosteum- a surface for all seasons. Osteop Int 18: 123-128.

Sencimen M, Aydintug YS, Ortakoglu K, Karslioglu Y, Gunhan O, Gunaydin Y (2007) Histomorphometrical analysis of new bone obtained by distraction osteogenesis and osteogenesis by periosteal distraction in rabbits. Int J Oral Maxillofac Surg 36: 235-242.

Simon TM, Van Sickle DC, Kunishima DH, Jackson DW (2003) Cambium cell stimulation from surgical release of the periosteum. J Orthop Res 21: 470-480.

Skerry TM (2006) One mechanostat or many? Modifications of the site-specific response of bone to mechanical loading by nature and nurture. J Musculoskelet Neuronal Interact 6: 122-127.

Solchaga LA, Cassiede P, Caplan AI (1998) Different response to osteo-inductive agents in bone marrow- and periosteum-derived cell preparations. Acta Orthop Scand 69: 426-432.

Squier CA, Ghoneim S, Kremenak CR (1990) Ultrastructure of the periosteum from membrane bone. J Anat 171: 233-239.

Termaat MF, Den Boer FC, Bakker FC, Patka P, Haarman HJThM (2005) Bone Morphogenetic Proteins: Development and Clinical Efficacy in the Treatment of Fractures and Bone Defects. J Bone Joint Surg 87: 1367-1378.

Tsubota S, Tsuchiya H, Shinokawa Y, Tomita K, Minato H (1999) Transplantation of osteoblast-like cells to the distracted callus in rabbits. J Bone Joint Surg 81-B: 125-129.

Uchiyama E, Yamakoshi K, Sasaki T (1998) Measurement of Mechanical Charateristics of Tibial Periosteum and Evaluation of Local Differences. J Biomech Eng 120: 85-91.

Vanderschueren D, Venken K, Ophoff J, Bouillon R, Boonen S (2006) Clinical Review: Sex Steroids and the Periosteum- Reconsidering the Roles of Androgens and Estrogens in Periosteal Expansion. J Clin Endocrinology and Metabolism 91: 378-382.

Volpin G, Rees JA, Ali SY, Bentley G (1986) Distribution of Alkaline Phosphatase Activity in Experimentally Produced Callus in Rats. J Bone Min Res 68-B:629-634.

Warrell E, Taylor JF (1979) The role of periosteal tension in the growth of long bones. J Anat 128(1):179-184.

Wilson-MacDonald J, Houghton GR, Bradley J, Morscher E (1990) The Relationship Between Periosteal Division and Compression or Distraction of the Growth Plate An Experimental Study in the Rabbit. J Bone Joint Surg 72-B: 303-308.

Zheng Y, Ringe J, Liang Z, Loch A, Chen L, Sittinger M (2006) Osteogenic potential of

human periosteum-derived progenitor cells in PLGA scaffold using allogenic serum. J Zhejiang Univ Science B 10: 817-824.

BIOGRAPHICAL INFORMATION

Phillip Daniel Warren was born in Arlington, VA, in 1982. He received his B.S. degree in Mechanical Engineering from the Georgia Institute of Technology, Atlanta, GA, 2005. He received his M.S. degree in Biomedical Engineering from the University of Texas, Arlington, TX, 2008. He has worked a few places and now intends to pursue a Ph.D. out in the desert, after which he wishes to join the Peace Corps and resume the gypsy lifestyle he used to enjoy as a younger man. His academic interest is in soft tissue mechanics and device design. He has no intention of growing up, wearing a tie, or combing his hair, ever.